Inorganic Chemistry
Cite This: Inorg. Chem. XXXX, XXX, XXX−XXX
Article
pubs.acs.org/IC

Photolytic Properties of Antivitamins B_{12}

Piotr Lodowski,[†] Megan J. Toda,[‡] Karolina Ciura,[†] Maria Jaworska,[†] and Pawel M. Kozlowski*[,‡,§]

[†]Department of Theoretical Chemistry, Institute of Chemistry, University of Silesia in Katowice, Szkolna 9, PL-40 006 Katowice, Poland

[‡]Department of Chemistry, University of Louisville, 2320 South Brook Street, Louisville, Kentucky 40292, United States

[§]Department of Food Sciences, Medical University of Gdansk, Al. Gen. J. Hallera 107, 80-416 Gdansk, Poland

Supporting Information

ABSTRACT: Antivitamins B_{12} represent an important class of vitamin B_{12} analogues that have gained recent interest in several research areas. In particular, 4-ethylphenylcobalamin (EtPhCbl) and phenylethynylcobalamin (PhEtyCbl) exemplify two such antivitamins B_{12} which have been characterized structurally and chemically. From a spectroscopic point of view, EtPhCbl is photolabile with a very low quantum yield of photoproducts, while PhEtyCbl is incredibly photostable. Herein, DFT and TD-DFT computations are provided to explore the photolytic properties of these compounds to shed light on the electronic properties that are indicative of these differences. Potential energy surfaces (PESs) were constructed to investigate the mechanisms of photodissociation leading to radical pair (RP) formation and the mechanisms of deactivation to the ground state. The S_1 PESs for each antimetabolite contain two energy minima, one being the metal-to-ligand charge transfer (MLCT) and another the ligand-field (LF) state. There are two possible pathways for photodissociation that can be identified for EtPhCbl but only one (path B) is energetically feasible and involves the lengthening of the Co−N_{Im} bond through the MLCT region followed by the lengthening of the Co−C bond through the LF region. For PhEtyCbl, there is not an energetically favorable path for photolysis; rather, internal conversion (IC) is the significantly preferred photophysical event.

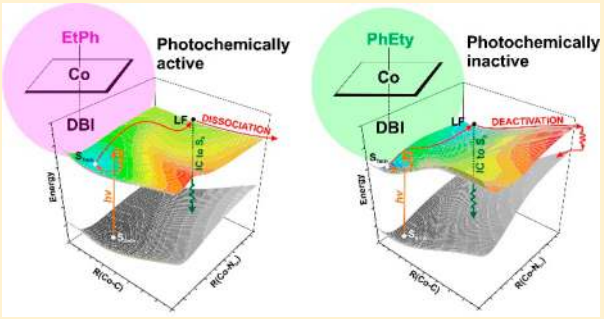

1. INTRODUCTION

Antivitamins are unique metabolites that are structurally similar to their respective vitamin analogues yet they counteract the physiological effects of those counterparts by various types of inhibition.[1−3] Despite their inhibitory nature, antivitamins can have useful medicinal applications.[4] For instance, vitamin K antagonists are used to reduce blood clotting by preventing thrombosis.[5,6] Researchers have begun to investigate, antivitamins B_{12}, which are structurally similar to vitamin B_{12} and other cobalamins (Figure 1), to unearth whether medical or biological applications are possible.[7,8] Recently, two antivitamins B_{12}, 4-ethylphenylcobalamin (EtPhCbl) and phenylethynylcobalamin (PhEtyCbl), have been synthesized and are structurally similar to the relevant B_{12} derivatives (Figure 1) involved in enzymatic catalysis.[9,10] EtPhCbl and PhEtyCbl differ from other known B_{12} antagonists in that they bind well to the proteins of the human B_{12}-transport system including intrinsic factor (IF), haptocorrin (HC), or transcobalamin (TC).[9,10] They can also bind to the B_{12}-processing protein CblC. EtPhCbl and PhEtyCbl are unaffected in this environment and do not convert to the biologically active B_{12}-cofactors, methylcobalamin (MeCbl) or adenosylcobalamin (AdoCbl), as is the case when cyanocobalamin (CNCbl) is bound to CblC.[9−11] This new class of organometallic cobalamins offers opportunities to explore B_{12} chemistry and the pathophysiological implications associated with the metabolism of B_{12} in humans further.

Both EtPhCbl and PhEtyCbl maintain all of the key structural features of cobalamins, with the exception being the nature of the upper axial ligand (Figure 1). For the biochemically important derivatives of B_{12}, CNCbl, MeCbl, and AdoCbl, the upper axial ligands are cyano, methyl, and adenosyl groups, respectively.[12,13] In the case of the antivitamins B_{12}, EtPhCbl and PhEtyCbl, the upper axial ligands are 4-ethylphenyl (EtPh) and 2-phenylethynyl (PhEty), respectively (Figure 1). The other structural features of cobalamins, including the antivitamins B_{12} understudy, are as follows. They contain a cobalt atom that is coordinated to the four inner nitrogens of a corrin macrocycle. The cobalt is also coordinated to two additional ligands in the Co(III) form known as the upper and lower axial ligands. For the lower axial ligand, the cobalt is coordinated to a nitrogen of the DBI base (DBI = dimethylbenzimidazole) in the base-on form or in certain enzymatic environments it is coordinated to a nitrogen of a histidine (His) in the base-off/His-on configuration. The upper axial ligand, described earlier, is variable and is used to distinguish cobalamin derivatives from each other.[12] Beyond

Received: April 9, 2018

DOI: 10.1021/acs.inorgchem.8b00956
Inorg. Chem. XXXX, XXX, XXX−XXX

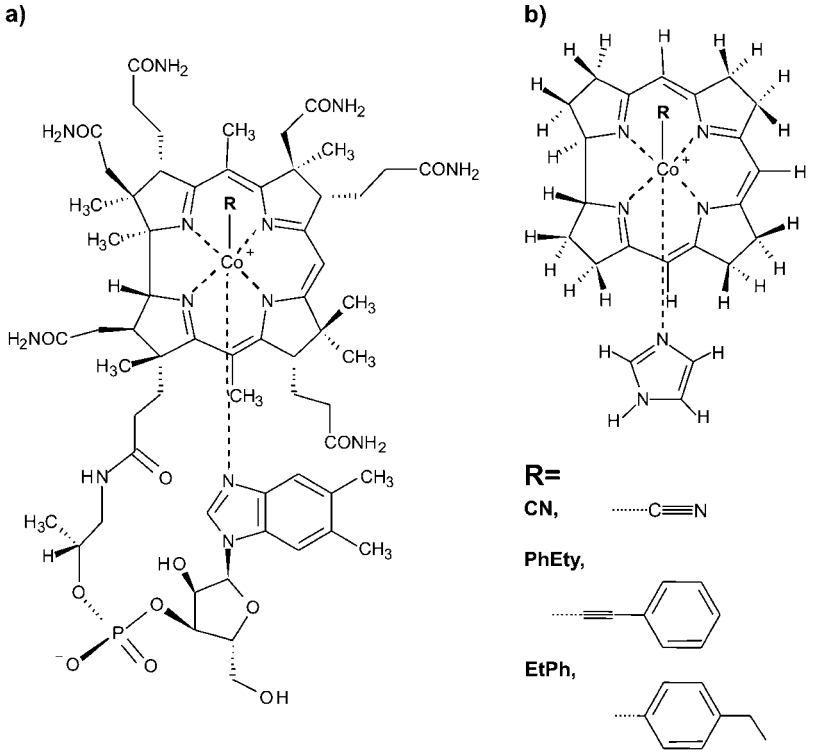

Figure 1. (a) Molecular structure of vitamin B_{12} (CNCbl, R = CN), phenylethynylcobalamin (PhEtyCbl, R = PhEty), and 4-ethylphenylcobalamin (EtPhCbl, R= EtPh). (b) Structure of model complex used in calculations (Im-[Co^{III}(corrin)]-R^+, R= PhEty and EtPh).

these structural details, EtPhCbl and PhEtyCbl also have unique properties from both a biochemical and spectroscopic perspective.

EtPhCbl is the first organometallic aryl cobalamin and is non-natural and chemically inert.[9] EtPhCbl has been used to induce functional vitamin B_{12} deficiency, also known as pernicious anemia, in laboratory mice.[14] EtPhCbl has also been called a conditional antivitamin B_{12} because despite the difficulty in cleaving the Co−C bond in the enzymatic environment it is possible to cleave this bond with light, albeit with a very low quantum yield of photoproducts.[15] This has been determined experimentally through advanced spectroscopic techniques[15] and has been confirmed in our preliminary theoretical investigations of EtPhCbl.[16] Transient absorption studies have indicated that photolysis results in the formation of cob(II)alamin although with a low quantum yield of <1%.[15]

PhEtyCbl represents an organometallic alkynylcobalamin (alkynyl-Cbl) which is structurally similar to CNCbl and is stable both thermally and photochemically.[10] Alkynyl-Cbls may be representative of an entire group of B_{12} derivatives that are photostable. From a spectroscopic point of view, PhEtyCbl is photostable, and the Co−C bond to the upper axial ligand does not cleave in the presence of light. This has been determined using transient absorption studies.[15]

The divergent photochemical properties of these two antimetabolites provide an opportunity for theoretical insights. Understanding the mechanism of photodissociation for a conditional antivitamin B_{12} like EtPhCbl, and conversely why PhEtyCbl is so remarkably photostable, is the motivation behind this present study. This work is a follow-up to our recent theoretical contribution,[16] which described preliminary computational results for the photodissociation of EtPhCbl where ground and excited state potential energy surfaces (PESs) were used to determine the most energetically favorable path for photolysis. This study provides a more detailed analysis of the photochemical properties of both of these antivitamins B_{12} including further insights into the mechanisms of photodissociation of the upper axial ligand. This theoretical perspective can be used to guide future experimental work in the area of B_{12} photochemistry while offering important insights into the electronic structure properties that facilitate photolability as well as those that are representative of photostability. The presented results are crucial in the context of designing aryl- and alkynl- cobalamins that are suitable agents for use in light-activated pharmaceutical applications.

2. COMPUTATIONAL DETAILS

The structural models were derived from X-ray crystallographic data available for EtPhCbl and PhEtyCbl.[9,10] The full structures of antivitamins were truncated to reduce computational cost. The side chains of the corrin macrocycle were replaced with hydrogens and the axial base was simplified by replacing the DBI axial ligand with imidazole (Im) (Figures 1 and S1). The nucleotide loop contains a phosphate ion (PO_4^-), so when this was removed, the truncated model had a positive charge. The geometries corresponding to the EtPhCbl and PhEtyCbl model complexes are denoted Im-[Co^{III}(corrin)]-$EtPh^+$ and Im-[Co^{III}(corrin)]-$PhEty^+$, respectively. These models are analogous to the base-on form. In the models for the base-off forms, the Im ligand is removed, and these structures are labeled as [Co^{III}(corrin)]-$EtPh^+$ and [Co^{III}(corrin)]-$PhEty^+$. A full molecular skeleton of both antivitamins and structures of model complexes are presented in Figure S1 for comparison.

The calculations for this study were all carried out using density functional theory (DFT)[17] and time-dependent DFT (TD-DFT),[18] employing resolution of identity (RI)[19] with the GGA-type BP86 functional[20,21] and the TZVPP basis set for Co, C, N, and the TZVP basis set for H.[22,23] In addition, the

DOI: 10.1021/acs.inorgchem.8b00956
Inorg. Chem. XXXX, XXX, XXX−XXX

Table 1. Selected Geometric Parameters of Base-On and Base-Off Forms of Im-[Co^{III}(corrin)]-$EtPh^+$ and Im-[Co^{III}(corrin)]-$PhEty^+$ Model Complexes for Optimized Geometries in the Ground State S_0 and in the Excited State S_1[a,b]

	Im-[Co^{III}(corrin)]-$EtPh^+$ base-on			[Co^{III} (corrin)]-$EtPh^+$ base-off		
parameter	S_0	exp.[a]	S_{1min}	S_0	$S_{1\,(min1)}$	$S_{1\,(min2)}$
		r[Å]			r[Å]	
Co - C_{1Ph}	1.973	1.981	1.927	1.939	1.847	2.018
Co - N_{Im}	2.197	2.230	2.107			
	Valence angle [deg]			Valence angle [deg]		
C_{1Ph}-Co - N_{Im}	179.4	176.5	171.1			
N_{21} - Co – N_{23}	171.7	172.9	170.9	164.7	155.6	145.8
N_{22} - Co – N_{24}	173.4	171.6	172.8	171.1	167.6	171.1
	Dihedral angle [deg]			Dihedral angle [deg]		
N_{21} – N_{22} – N_{23} - Co	-3.9	-3.6	-4.3	-10.0	-16.6	-23.1
	Im-[Co^{III}(corrin)]-$PhEty^+$ base-on			[Co^{III}(corrin)]-$PhEty^+$ base-off		
parameter	S_0	exp.[b]	S_{1min}	S_0	S_{1min}	
		r[Å]			r[Å]	
Co – C_{1Ety}	1.860	1.861	1.775	1.820	1.857	
Co - N_{Im}	2.084	2.084	2.057			
	Valence angle [deg]			Valence angle [deg]		
C_{1Ety}-Co - N_{Im}	179.2	178.6	178.7			
N_{21} - Co – N_{23}	173.0	173.4	170.7	165.5	148.0	
N_{22} - Co – N_{24}	172.3	172.1	172.6	172.0	168.8	
	Dihedral angle [deg]			Dihedral angle [deg]		
N_{21} – N_{22} – N_{23} - Co	-1.9	-0.5	-4.0	-9.3	-21.9	

[a]Ref 9. [b]Ref 10.

Conductor-like Screening Model (COSMO) with water as the solvent was employed.[24] All calculations were completed using the TURBOMOLE software[25] with the exception of the lambda (Λ) parameter calculations which were obtained with the GAMESS program.[26]

This level of theory has been applied successfully in several of our previous studies.[27−32] In particular, there is a complete explanation of our confidence in the methodology in our recent communication that discussed preliminary results for the photodissociation of EtPhCbl.[16] One of the important conclusions from these previous studies was that BP86 is an appropriate functional to use in calculations of excited states for cobalamin systems. This was also confirmed by benchmark studies for MeCbl and cyanocobalamin, CNCbl.[33−35] Interestingly, in the benchmark analysis for MeCbl, where the TD-DFT results were compared to *ab initio* calculations using methods such as CASSCF/MC-XQDPT2 and EOM-CCSD, it was found that hybrid functionals incorrectly described the character of the S_1 state.[33] The commonly used hybrid functionals give predominantly $\pi \rightarrow \pi^*$ character of the $S_0 \rightarrow S_1$ transition, as opposed to the metal-to-ligand charge transfer (MLCT) interpretation indicated by the high-level wave function approaches. Otherwise, pure GGA functionals, like BP86, described the S_1 state as MLCT $d/\pi \rightarrow \pi^*$ excitation, which is completely consistent with the *ab initio* calculations.[33] It should be emphasized that for various cobalamins, MLCT character of the S_1 excited state has been also confirmed experimentally.[36−39]

In regards to the potential for underestimation of long-range charge-transfer (CT) type excitations energies, Λ parameters have been calculated.[40] These calculations were used to determine whether or not CT-type excitation energies are underestimated. If excitation energies are underestimated, then it is likely due to poor overlap between the occupied and virtual orbitals involved in the transition. The Λ diagnostic results, in the range from 0 to 1, can indicate whether or not poor overlap persists between orbitals involved in the electronic excitation. For GGA-type functionals, if Λ is less than 0.4, then excitations are likely to be significantly underestimated; conversely, if Λ is greater than 0.4, then excitations are most likely not underestimated. The results from the Λ diagnostic calculations shown in Tables 2 and 3 have provided us with the confidence that CT-type excitation energies are not significantly underestimated in the investigated antivitamin systems.

3. RESULTS AND DISCUSSION

3.1. Structural Properties of Antivitamins. Selected geometric parameters of the S_0 and S_1 optimized structures for the base-on and base-off forms of EtPhCbl and PhEtyCbl model complexes are gathered in Table 1. A more detailed list of the geometric parameters for the coordination sphere of cobalt are provided in Tables S1 and S2. The optimized structures of the model species are presented in Figures S2 and S3.

For the base-on form of both model complexes, the optimized S_0 structural parameters were compared to the corresponding parameters in the crystal structures. The axial bond lengths, valence angles, and the dihedral angles around the coordination sphere of cobalt all showed good agreement between the optimized geometries and the crystal structures.

DOI: 10.1021/acs.inorgchem.8b00956
Inorg. Chem. XXXX, XXX, XXX−XXX

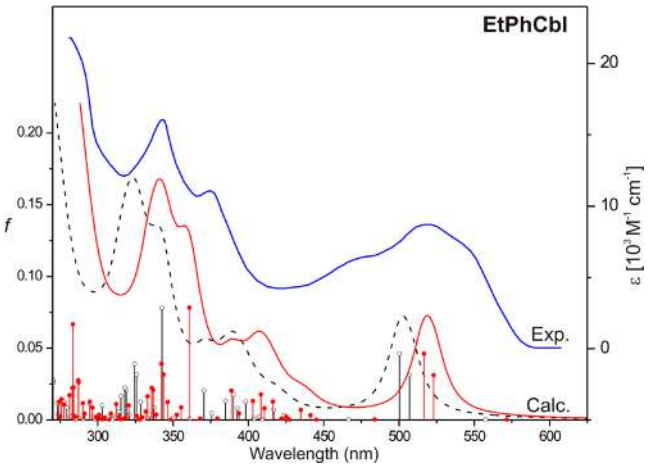

Figure 2. Experimental (blue line) and the TD-DFT simulated absorption spectra for Im-[Co^{III}(corrin)]-$EtPh^+$ model complex: not scaled (black lines) and scaled (red lines) with $\alpha(S_3)$ and $\gamma(S_{25})$. Simulation is based on TD-DFT/BP86 calculations in water solution. Experimental spectrum is from ref 15.

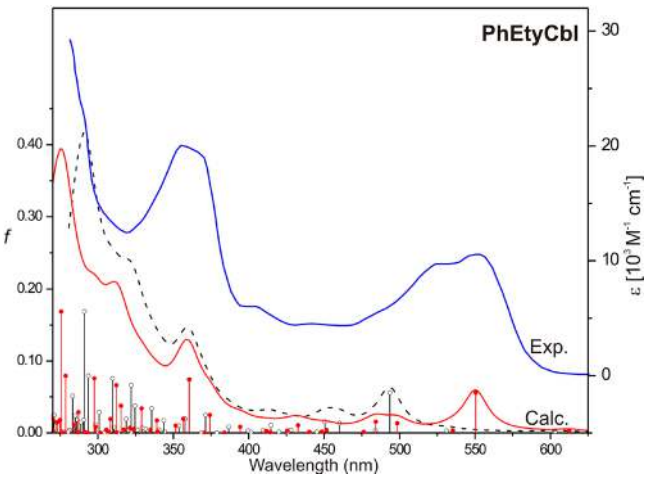

Figure 3. Experimental (blue line) and the TD-DFT simulated absorption spectra for Im-[Co^{III}(corrin)]-$PhEty^+$ model complex: not scaled (black lines) and scaled (red lines) with $\alpha(S_3)$ and $\gamma(S_{19})$. Simulation is based on TD-DFT/BP86 calculations in water solution. Experimental spectrum is from ref 15.

For Im-[Co^{III}(corrin)]-$EtPh^+$, the optimized axial bond lengths are 1.973 and 2.197 Å for the Co−C_{1Ph} and Co−N_{Im}, respectively. In the crystal structure, these bonds are 1.981 and 2.230 Å. For Im-[Co^{III}(corrin)]-$PhEty^+$, the optimized bond lengths of the Co−C_{1Ety} and Co−N_{Im} axial bonds are 1.860 and 2.084 Å, respectively. In the crystal structure these bonds are 1.861 and 2.084 Å. The axial bonds in the optimized geometries of the lowest singlet excited state (S_{1min}) are slightly shorter compared to the geometry of the S_0. Shortening of the axial bonds is observed for both of the S_1 model complexes. The optimized geometry of the S_0 for the base-off models is also characterized by a small shortening of the Co−C axial bond in comparison to the S_0 for the base-on form. According to the results from Table 1, the length of Co−C_{1Ph} and Co−C_{1Ety} axial bonds is 1.939 and 1.820 Å for [Co^{III}(corrin)]-$EtPh^+$ and [Co^{III}(corrin)]-$PhEty^+$, respectively. Generally, for the base-on and base-off forms of both antivitamins, the calculated valence and dihedral angles from the optimizations showed good agreement with experiment (Table 1). However, it should be noted that for the S_0 and S_1 optimized geometries, the coordination sphere of the base-off form is more distorted. This is clearly visible when comparing the N_{21}−Co−N_{23} and N_{21}−N_{22}−N_{23}−Co angle values between the base-off and base-on forms of the model complexes. For the base-off forms, the valence angles (N_{21}−Co−N_{23}) are smaller, whereas the dihedral angles (N_{21}−N_{22}−N_{23}−Co) are larger in comparison to those of base-on form (Table 1).

3.2. Absorption Spectra of Antivitamins. Cobalamins have characteristic features in their absorption spectra.[12,13,41−43] Particularly for CNCbl, which has been referred to as the "paradigm system" for studying the electronically excited states of cobalamins, there are two distinctive bands including the γ and α/β bands.[44] The γ band (360 nm) is located in the UV part of the absorption spectrum, whereas the α/β band, with a maximum at 550 nm, occurs in the visible region. The α/β bands arise primarily from the $\pi \rightarrow \pi^*$ transition, and the α-band is more intense than the β band.[13] Alkyl-cobalamins such as MeCbl and AdoCbl differ in their UV−visible spectra when compared to the "typical" CNCbl spectrum.[41] In the region of the α/β band, the β-band is more intense. PhEtyCbl has an α/β band that is similar to that of CNCbl and has a very pronounced γ band.[15] EtPhCbl's α/β band is blue-shifted and is more similar to AdoCbl's UV−visible spectrum.[15]

To obtain the electronic spectra, 25 singlet electronic transitions were calculated using TD-DFT from the S_0 optimized geometries. The calculated excitations (black lines) along with the corresponding simulated absorption spectra are shown in Figure 2 and 3. In order to allow a comparison with the simulations, the experimental absorption spectra (blue lines) are also presented in the figures. The simulated spectra for both models of antivitamins are slightly shifted by about 25−50 nm in the direction of higher energy in relation to experiment. Such a shift, as a consequence of an overestimation of transition energy, is characteristic of TD-DFT results for nonalkyl cobalamins, e.g., CNCbl.[34] Despite this, the resulting shape of the simulated spectral lines are very similar to the experimental spectra. For both model complexes, the simulated spectra have a visible band in the range from ∼450 to ∼550 nm which can be assigned to the α/β band from experiment. In this range, the simulated spectrum for Im-[Co^{III}(corrin)]-$EtPh^+$ contains four singlet electronic transitions, S_1−S_4. For the second model, Im-[Co^{III}(corrin)]-$PhEty^+$, the low energy part of calculated spectrum is determined by six excitations, S_1−S_6. The calculated transitions in the range of the α/β band have different values for the oscillator strength, but one transition (S_3) in the case of Im-[Co^{III}(corrin)]-$PhEty^+$ and two transitions (S_2 and S_3) in the case of Im-[Co^{III}(corrin)]-$EtPh^+$ have relatively large intensity. The remaining transitions have medium or very small oscillator strengths. It is worth mentioning that in the case of both model complexes there are low-lying excited states for which electronic transitions have very small oscillator strengths. Two such transitions at 603 and 531 nm and one at 557 nm exist for Im-[Co^{III}(corrin)]-$PhEty^+$ and Im-[Co^{III}(corrin)]-$EtPh^+$, respectively. These transitions are very interesting because they can play a crucial role in photochemical processes.

The second characteristic band for cobalamins, the γ band, can be also identified in the simulated electronic spectra, especially for Im-[Co^{III}(corrin)]-$EtPh^+$. The two maxima between 300 nm -360 nm in the simulated spectrum of the Im-[Co^{III}(corrin)]-$EtPh^+$ can be ascribed to the two separated

DOI: 10.1021/acs.inorgchem.8b00956
Inorg. Chem. XXXX, XXX, XXX−XXX

Table 2. Four Lowest, Vertical Singlet States and the $S_1 \rightarrow S_0$ Transition for Im-[Co^{III}(corrin)]-$EtPh^+$ and [Co^{III}(corrin)]-$EtPh^+$ Model Complexes

	E [eV]	λ [nm]	f	Λ[a]	%	character		exp. λ [nm] (eV)
					Im-[Co^{III}(corrin)]-$EtPh^+$ (Base-On)			
S_1	2.22	557.5	0.0002	0.541	50.9	H-1 → L	$\pi + d_{xz} \rightarrow \pi^*$	
					46.3	H-2 → L	$d_{xz} + \pi_{Ph} \rightarrow \pi^*$	
S_2	2.44	506.9	0.0314	0.712	73.5	H → L	$d_{yz} + \pi \rightarrow \pi^*$	525 (2.36)
					11.8	H-1 → L	$\pi + d_{xz} \rightarrow \pi^*$	
S_3	2.48	500.3	0.0462	0.550	46.4	H-2 → L	$d_{xz} + \pi_{Ph} \rightarrow \pi^*$	
					34.6	H-1 → L	$\pi + d_{xz} \rightarrow \pi^*$	
					11.3	H → L	$d_{yz} + \pi \rightarrow \pi^*$	
S_4	2.66	466.6	0.0004	0.302	97.2	H-3 → L	$d_{x^2-y^2} \rightarrow \pi^*$	
S_{1min}	1.72	720.4	0.0015	0.490	96.6	H → L	$d_{xz} + \pi_{Ph} \rightarrow \pi^*$ (MLCT/LL)	
					[Co^{III}(corrin)]-$EtPh^+$ (Base-Off)			
S_1	2.19	566.8	0.0006	0.506	81.8	H-1 → L	$\pi_{Ph} + d_{xz} \rightarrow \pi^*$	
					14.8	H → L+1	$d_{yz} + \pi \rightarrow \sigma^*(d_z^2)$	
S_2	2.22	558.5	0.0064	0.532	62.3	H → L+1	$d_{yz} + \pi \rightarrow \sigma^*(d_z^2)$	
					13.6	H-1 → L	$\pi_{Ph} + d_{xz} \rightarrow \pi^*$	
					13.5	H → L	$d_{yz} + \pi \rightarrow \pi^*$	
S_3	2.33	531.3	0.0040	0.567	84.9	H-1 → L+1	$\pi_{Ph} + d_{xz} \rightarrow \sigma^*(d_z^2)$	
S_4	2.42	512.7	0.0307	0.698	67.4	H → L	$d_{yz} + \pi \rightarrow \pi^*$	
					13.4	H → L+1	$d_{yz} + \pi \rightarrow \sigma^*(d_z^2)$	
$S_{1(min1)}$	1.68	738.8	0.0019	0.482	92.9	H → L	$(d_{xz} + d_{yz}) + \pi_{Ph} \rightarrow \pi^*$ (MLCT/LL)	
$S_{1(min2)}$	1.40	888.1	0.0013	0.612	99.0	H → L	$(d_{xz} + d_{yz}) + \pi_{Ph} \rightarrow \sigma^*(d_z^2)$ (LF)	

[a] Λ parameters were obtained from TD-DFT/BP86/TZVPP calculations with use Gamess quantum chemistry program.

Table 3. Four Lowest, Vertical Singlet States and the $S_1 \rightarrow S_0$ Transition for Im-[Co^{III}(corrin)]-$PhEty^+$ and [Co^{III}(corrin)]-$PhEty^+$ Model Complexes

	E [eV]	λ [nm]	f	Λ[a]	%	character		exp. λ [nm] (eV)
					Im-[Co^{III}(corrin)]-$PhEty^+$ (Base-On)			
S_1	2.05	603.1	0.0019	0.459	93.2	H → L	$\pi_{PhEty} + d_{yz} \rightarrow \pi^*$	
S_2	2.33	531.1	0.0029	0.610	59.9	H-2 → L	$\pi_{Ety} + d_{yz} \rightarrow \pi^*$	
					22.6	H-1 → L	$\pi + d_{z^2} \rightarrow \pi^*$	
					14.3	H-3 → L	$\pi_{Ety} + d_{yz} + \pi \rightarrow \pi^*$	
S_3	2.51	493.6	0.0558	0.609	66.5	H-1 → L	$\pi + d_{z^2} \rightarrow \pi^*$	550 (2.25)
					21.6	H-2 → L	$\pi_{Ety} + d_{yz} \rightarrow \pi^*$	
S_4	2.56	483.9	0.0034	0.460	87.9	H → L+1	$\pi_{PhEty} + d_{yz} \rightarrow d_{xy} - n$	
S_{1min}	1.59	777.9	0.0008		97.6	H → L	$\pi_{PhEty} + d_{yz} \rightarrow \pi^*$ (MLCT/LL)	
					[Co^{III}(corrin)]-$PhEty^+$ (Base-Off)			
S_1	1.64	756.9	0.0006	0.528	99.3	H → L	$\pi_{PhEty} + d_{yz} \rightarrow \sigma^*(d_z^2) - n$	
S_2	1.94	637.5	0.0017	0.444	93.0	H → L+1	$\pi_{PhEty} + d_{yz} \rightarrow \pi^*$	
S_3	2.03	609.5	0.0022	0.590	96.3	H-1 → L	$\pi_{Ety} + d_{yz} \rightarrow \sigma^*(d_z^2) - n$	
S_4	2.29	541.3	0.0021	0.600	74.9	H-1 → L+1	$\pi_{Ety} + d_{yz} \rightarrow \pi^*$	
					14.1	H-2 → L	$\pi_{Ety} + \pi + d_{xz} \rightarrow \sigma^*(d_z^2) - n$	
S_{1min}	0.98	1259.8	0.0002		99.8	H → L	$\pi_{PhEty} + d_{xz} \rightarrow \sigma^*(d_z^2) - n$ (LF)	

[a] Λ parameters were obtained from TD-DFT/BP86/TZVPP calculations which use Gamess quantum chemistry program.

peaks that are observed in the γ band region of the experimental spectrum. The transition with the largest oscillator strength in this part of the calculated spectrum is S_{19} at 343 nm (Table S3) and can be attributed to the first peak at ~375 nm in the experimental spectrum. The second peak, which is apparent both in the simulated and experimental spectrum, is a superposition of several close electronic transitions, S_{24}–S_{29}, which have moderate oscillator strength. Two of them, S_{24} at 326 nm and S_{25} at 324 nm (Table S3), should have the greatest impact on the location and intensity of the second peak in the γ region. For Im-[Co^{III}(corrin)]-$PhEty^+$, the γ band is less pronounced in the simulated spectrum because the intensity of this band is not well reproduced in calculations. The experimental γ band reasonably correlates to the maximum of the simulated spectrum located between ~345 nm and ~390 nm. In this range, nine electronic transitions S_{15}–S_{23} are identifiable (Table S5). The excitations forming the γ band have rather moderate or small oscillator strengths except for one transition at 360 nm. This transition (S_{19}) has a large oscillator strength value (f = 0.0742) and correlates with the maximum of the experimental γ band.

To further improve the agreement between experiment and theory, we applied a scaling procedure to the electronic transitions. The calculated spectra of both investigated model complexes were scaled according to the procedure given in our previous study (see eq 1 of ref 45). For each spectrum, an optimal set of two scaling parameters, ζ and E_{Shift}, were determined under the assumption that the energies of the

DOI: 10.1021/acs.inorgchem.8b00956
Inorg. Chem. XXXX, XXX, XXX–XXX

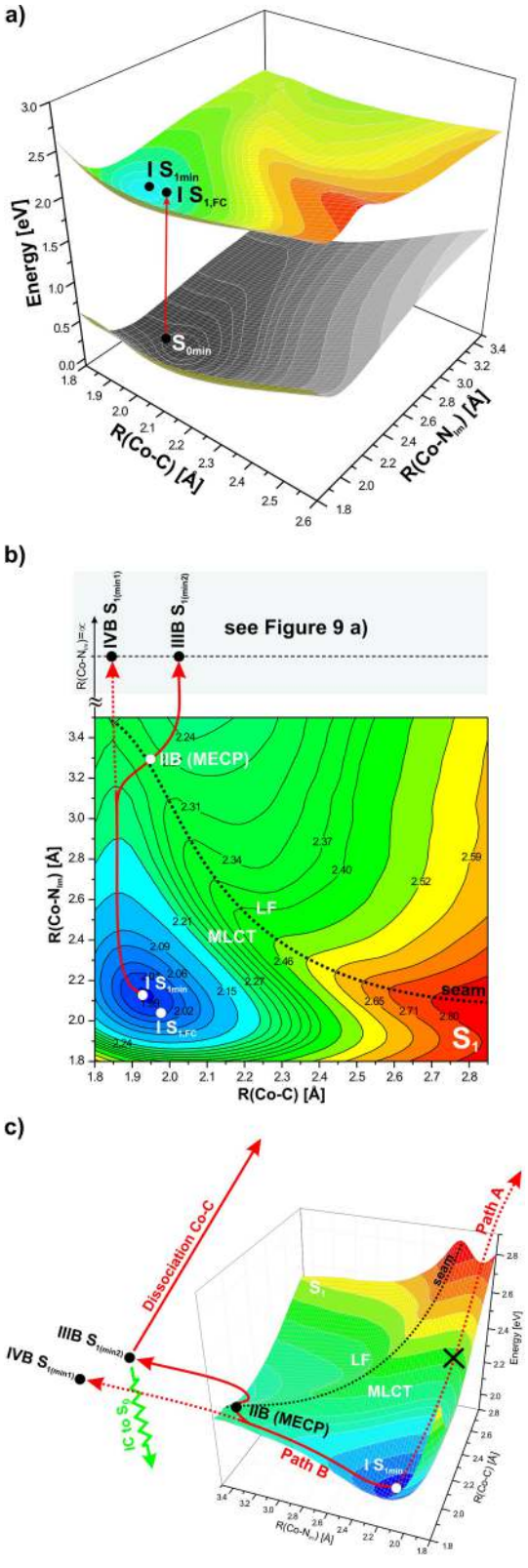

Figure 4. (a) Potential energy surfaces as a function of axial bond lengths for optimized geometry of the ground state S_0 and optimized geometry of the S_1 excited state of Im-[Co^{III}(corrin)]-$EtPh^+$ model complex, (b) vertical projections of S_1 PES, (c) scheme of photoreaction for Im-[Co^{III}(corrin)]-$EtPh^+$ model complex.

electronic excitations associated with the α and γ bands should be reproduced precisely. The most intense $S_0 \rightarrow S_3$ transitions, at 500 and 494 nm for Im-[Co^{III}(corrin)]-$EtPh^+$ and Im-[Co^{III}(corrin)]-$PhEty^+$, respectively, were assigned to the maximum of lowest energy absorption band. For the γ band, several different transitions were tested to determine the optimal scaling parameters. On this basis, it has been concluded that the energy of the $S_0 \rightarrow S_{24}$ excitation at 324 nm for Im-[Co^{III}(corrin)]-$EtPh^+$ and the $S_0 \rightarrow S_{19}$ excitation at 360 nm for Im-[Co^{III}(corrin)]-$PhEty^+$ should be assigned to the maximum of the experimental γ band. The results for the scaled spectra are shown in Figures 2 and 3 (red lines). The simulated spectra for both model complexes are in good accordance with experiment and agree well in regards to the characteristic features of spectral line of cobalamins.

The electronic structures of the calculated excited states were obtained on the basis of analysis of the frontier Kohn−Sham molecular orbitals (KS MOs) involved in the TD-DFT electronic excitations. Figures S4 and S5 contain images of relevant molecular orbitals. The characters of the transitions for the four low-lying singlet excited states of Im-[Co^{III}(corrin)]-$EtPh^+$ and Im-[Co^{III}(corrin)]-$PhEty^+$ are presented in Tables 2 and 3, respectively. For Im-[Co^{III}(corrin)]-$EtPh^+$ the S_1 state is the result of electronic transitions from the HOMO−1 and HOMO−2 orbitals to the LUMO orbital, and this corresponds to the $\pi + d_{xz} \rightarrow \pi^*$ (51%) and $d_{xz} + \pi_{Ph} \rightarrow \pi^*$ (46%) excitations. Both of these excitations can be characterized as MLCT transitions. The S_1 transition for Im-[Co^{III}(corrin)]-$PhEty^+$ is also MLCT type and has been characterized as HOMO to LUMO, $\pi_{PhEty} + d_{yz} \rightarrow \pi^*$ (93%), excitation. The remaining low-lying singlet states for both species have similar character to the S_1 state. These states are mainly a result of $\pi/d \rightarrow \pi^*$ excitations, excluding the S_4 transition for Im-[Co^{III}(corrin)]-$PhEty^+$ which is $\pi/d \rightarrow d$ type. In the case of the base-off forms, the characters of the low energy transitions are rather diametrically opposed. The lowest singlet states are dominated by $\pi/d \rightarrow \sigma^*(d_{z^2})$ excitations, therefore the states are of predominantly the LF type. These results clearly show, that detachment of the axial base causes a change in the order of MLCT and LF states. Thus, unlike the base-on forms, the S_1 state of the base-off forms has mostly $d \rightarrow \sigma^*(d_{z^2})$ character.

For the optimized S_{1min} geometry of Im-[Co^{III}(corrin)]-$EtPh^+$, the excited state is HOMO → LUMO transition and has been characterized as $d_{xz} + \pi_{Ph} \rightarrow \pi^*$ (97%, MLCT/LL). For the base-off form, there are two S_1 minima, $S_{1(min1)}$ and $S_{1(min2)}$, and these are characterized as $(d_{xz} + d_{yz}) + \pi_{Ph} \rightarrow \pi^*$ (93%, MLCT/LL) and $(d_{xz} + d_{yz}) + \pi_{Ph} \rightarrow \sigma^*(d_{z^2})$ (99%, LF). Figure S6 depicts the HOMO and LUMO molecular orbitals for electron excitations in the optimized geometries of the S_1 states and cross-sectional contours of electron density difference between the S_1 and S_0 states for both forms of EtPhCbl. The S_{1min} for optimized geometry of Im-[Co^{III}(corrin)]-$PhEty^+$ is characterized as $\pi_{PhEty} + d_{yz} \rightarrow \pi^*$ excitation (98%, MLCT/LL). For [Co^{III}(corrin)]-$PhEty^+$ the S_{1min} is characterized as LF state and corresponds to the $\pi_{PhEty} + d_{xz} \rightarrow \sigma^*(d_z^2) - n$ transition (99%). A more complete listing of the lowest singlet states and their corresponding orbital characterizations can be found in Table S3 for Im-[Co^{III}(corrin)]-$EtPh^+$, Table S4 for [Co^{III}(corrin)]-$EtPh^+$, Table S5 for Im-[Co^{III}(corrin)]-$PhEty^+$, and Table S6 for [Co^{III}(corrin)]-$PhEty^+$.

3.3. Constructions of PESs and Energy Profiles. To explore the mechanism of Co−C bond photodissociation, PESs corresponding to the S_1 state were constructed as a function of axial bond lengths. These bonds experience the most significant changes upon electronic excitations while the corrin structure is

DOI: 10.1021/acs.inorgchem.8b00956
Inorg. Chem. XXXX, XXX, XXX−XXX

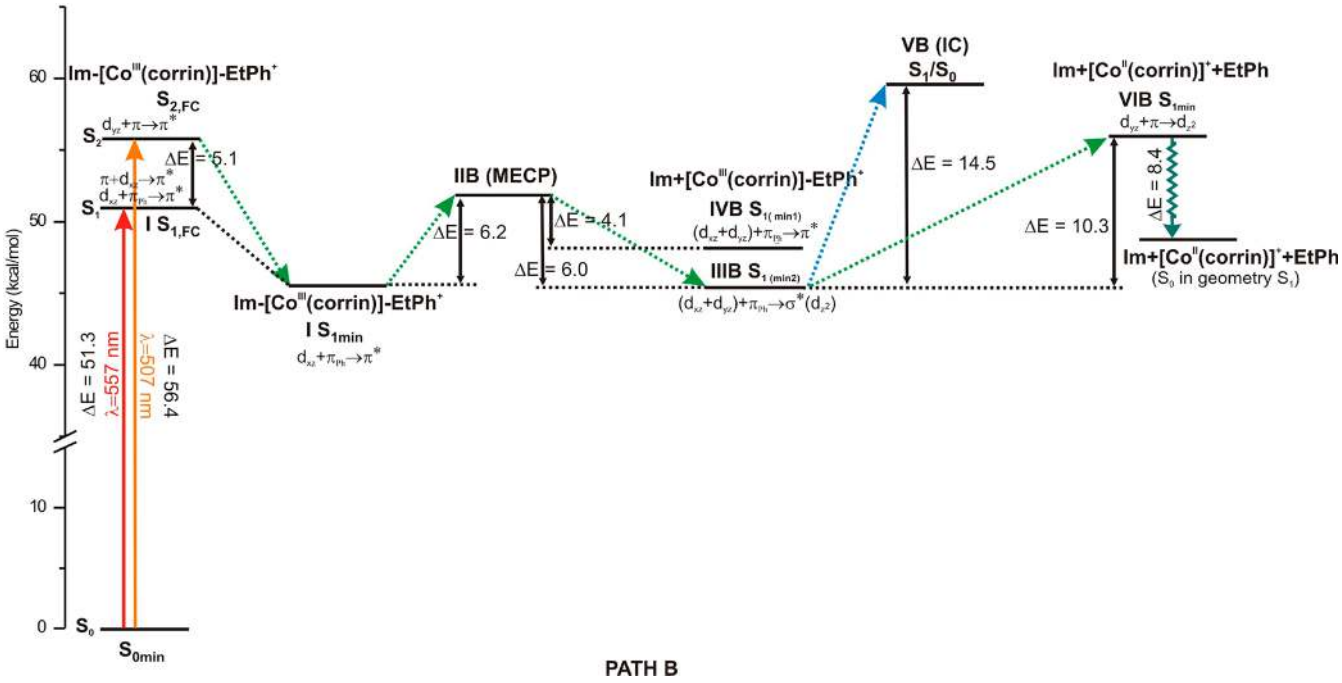

Figure 5. Energy diagram of photoreaction on path B for Im-[Co^{III}(corrin)]-$EtPh^+$ model complex (ΔE values in kcal/mol).

maintained. This has been shown theoretically and experimentally with XANES measurements reported for CNCbl.[27,46] The involvement of triplet states was not considered, based on magnetic effects measurements that suggest that this is unlikely.[47,48] Prior to constructing the S_1 surfaces, the S_0 PESs were constructed by optimizing the geometries associated with the structures resulting from the systematic elongation of the two axial bonds. The choice of methodology is further explained in the "Computational Details" section. The PESs for the low-lying S_1 and S_2 states of Im-[Co^{III}(corrin)]-$EtPh^+$ and Im-[Co^{III}(corrin)]-PhEty$^+$ were constructed from the manifold of vertical excitations (Figure S7). The relaxed PESs representing the S_1 state were obtained by optimizing the corresponding excited state geometries (Figures 4 and 6). Overall, comparison of the S_1 PESs based on vertical excitations (Figure S7) with the relaxed S_1 PESs (Figures 4 and 6) show that the surfaces do not significantly differ from each other.

3.4. Interpretation of Photochemical Data Based on PESs. Following our previous studies, we have developed a systematic approach to employ three-dimensional PESs to gain insights into the mechanism of photolability for cobalamins.[16,27−29,31] The PES of S_1 state for both antivitamin models have characteristic topology, similar to the S_1 PESs of other cobalamins. Basically, the shape of this surface is the result of the intersection between two surfaces of electronic states with different character, MLCT and LF. As a consequence, the surface of the lowest singlet state has two minima: One occurs for shorter axial bonds, while the second corresponds to elongated bonds. Photochemical conversion between the two minima regions requires overcoming an energetics barrier, with localization and height usually dependent upon the character of the upper axial ligand. Obviously, among the available photochemical paths, the preference is for the path with the smallest energetic barrier. The energetics profile of the photoreaction on the S_1 surface will be different for each path and depends on the initial reaction step from the MLCT minimum, i.e., from which the axial coordinate undergoes elongation first. There are two possible photoreaction pathways (paths A and B) that have been identified. Path A involves initially lengthening the Co−C bond from the MLCT I S_{1min} minimum, followed by the subsequent elongation of Co−N_{Im}. In contrast, path B involves the lengthening of the Co−N_{Im} bond through the MLCT region to the ligand field (LF) stationary point. The stable intermediate for path B involves a LF state responsible for Co−C bond dissociation. Conversion to the ground state prior to dissociation is possible via out-of-plane distortion of the corrin ring at the stationary point of the LF state. A second possible mechanism of internal conversion (IC) can engage deactivation of the electronically excited photoproduct [Co^{II}(corrin)]$^+$.[32]

From a theoretical point of view, regardless of whether Co−C photodissociation involves paths A or B, the result is the formation of the same RP products in the case of homolytic cleavage. The general RP products, for cobalamins include {N_{base}···[Co^{II}(corrin)]* + $^{\bullet}$R}, where N_{base}···[Co^{II}(corrin)]* (N_{base} can be DBI, Im, or water) denotes the electronically excited states of the cobalamin(II), while $^{\bullet}$R is the corresponding radical. It seems as though the Co−N_{base} bond does not ultimately break when the base-on configuration is present, but it is significantly elongated as the upper axial ligand dissociates. It also has been demonstrated that the Co−N_{base} distance controls the nature of the electronically excited states of the Co(II) species. However, whether or not the Co−C bond finally breaks is dependent upon the nature of the upper axial ligand.

3.5. EtPhCbl PES. The PESs gathered in Figures 4 and S7 show the locations of the energy minima for the S_0, S_1, and S_2 electronic states of Im-[Co^{III}(corrin)]-$EtPh^+$. The relaxed S_1 PES indicates two distinct regions that are low in energy that are delineated by a seam (Figure 4b,c). The first is located in the area of the projection corresponding to shorter Co−C and Co−N_{Im} bond lengths and is denoted by the point I S_{1min}. The second low energy region is located in the area of PES where Co−C distances are short and Co−N_{Im} distances are elongated.

DOI: 10.1021/acs.inorgchem.8b00956
Inorg. Chem. XXXX, XXX, XXX−XXX

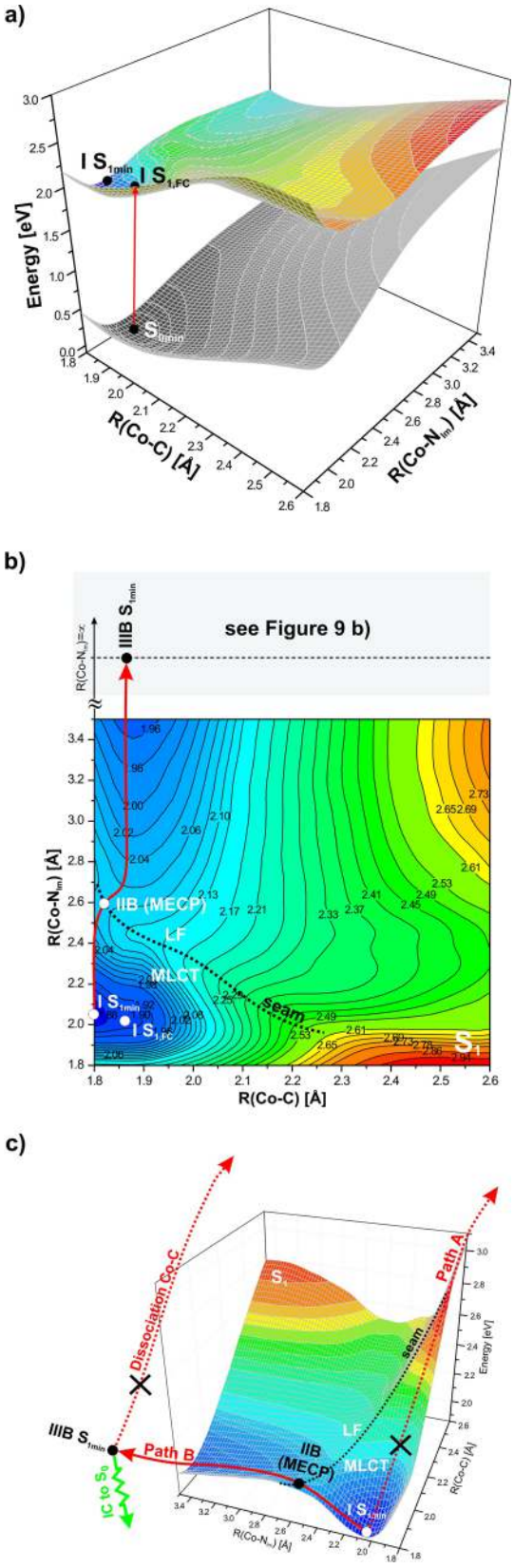

Figure 6. (a) Potential energy surfaces as a function of axial bond lengths for optimized geometry of the ground state S_0 and optimized geometry of the S_1 excited state of Im-[Co^{III}(corrin)]-PhEty$^+$ model complex, (b) vertical projections of S_1 PES, (c) scheme of photoreaction for Im-[Co^{III}(corrin)]-PhEty$^+$ model complex.

The highest energy for both the S_1 and S_2 states is found in the part of the surface that corresponds to the longest Co−C bond lengths and short Co−N bond lengths and this region is shown as a bright red color in the PESs gathered in Figures 4 and S7. The S_2 state has one particularly shallow energy minima in the region of shorter Co−C and longer Co−N_{Im} bond distances (Figure S7). On the S_1 surface, as shown in Figure 4c, there is a steep increase in energy as the Co−C bond is lengthened. This steep increase in energy is not observed as the Co−N_{Im} bond is lengthened simultaneously with Co−C. The S_1 minima regions result from the interaction of at least two different electronic states. The region associated with shorter Co−C axial bond lengths corresponds to MLCT transition, whereas the minimum associated with longer Co−C and Co−N_{Im} bonds corresponds to LF excitation, which has dominant cobalt d → d character. Charge transfer states for the elongated axial bond were not observed because the LF state primarily involves electronic excitation localized on the cobalt. Additionally, in Figure 4c, besides the minimum I S_{1min} in the MLCT region of the PES, several other stationary points in the LF part of surface are shown. IIB (MECP) denotes the minimum energy crossing point of path B. The two local minima on either side of the seam in the LF region are the MLCT minimum (IVB $S_{1(min1)}$) and the LF minimum (IIIB $S_{1(min2)}$), which correspond to the structure with the completely detached axial base from the cobalt center.

3.6. Photodissociation and Energy Profiles of EtPhCbl Photoreaction. In the case of Im-[Co^{III}(corrin)]-EtPh$^+$, photodissociation involving path A is ineffective as it is not energetically feasible due to the steep increase in energy. Conversely, path B is effective where elongation of the Co−N_{Im} bond initially involves the MLCT region up to the distance of ∼3.4 Å where crossing of the seam through the MECP, labeled as IIB, takes place. At this stage, the crossing between MLCT and LF electronic states is essentially barrierless, as discussed in more detail later, and the photoreaction further proceeds via elongation of the Co−C bond through the LF region. Consequently, the final dissociation of the Co−C bond would start from IIIB $S_{1(min2)}$ point. In addition to photodissociation, IC to S_0 may take place from LF minimum.

The energetics of the photoreaction along path B for the Im-[Co^{III}(corrin)]-EtPh$^+$ model complex is shown in Figure 5 for key points along the reaction path. Upon excitation at a wavelength of 557 nm promotion to the S_1 state will occur and simultaneously, excitation at 507 nm leads to population of the S_2 state. There is an energy difference of 5.1 kcal/mol between these two electronic levels (Figure 5). After vertical excitation, the system undergoes relaxation to the energy minimum of the lowest singlet state, thus on the photoreaction path, the first intermediate state corresponds to the minimum in the MLCT region, I S_{1min}. The photoreaction then leads to the MECP, requiring 6.2 kcal/mol. Outside the MECP point, in the area of the LF state there is a relaxation, which ends in IIIB $S_{1(min2)}$ stationary point. At this point of photoreaction, the stable intermediate in the excited state is created. From the IIIB minimum there is a competition between photodissociation and IC to the ground state. There is not a significant difference in the energy required to overcome the barrier for either of these processes. IC and photodissociation would require 14.5 and 10.3 kcal/mol, respectively (Figure 5), which suggests that both processes can be competitive. These theoretical insights also corroborate recent experimental findings.[15]

DOI: 10.1021/acs.inorgchem.8b00956
Inorg. Chem. XXXX, XXX, XXX−XXX

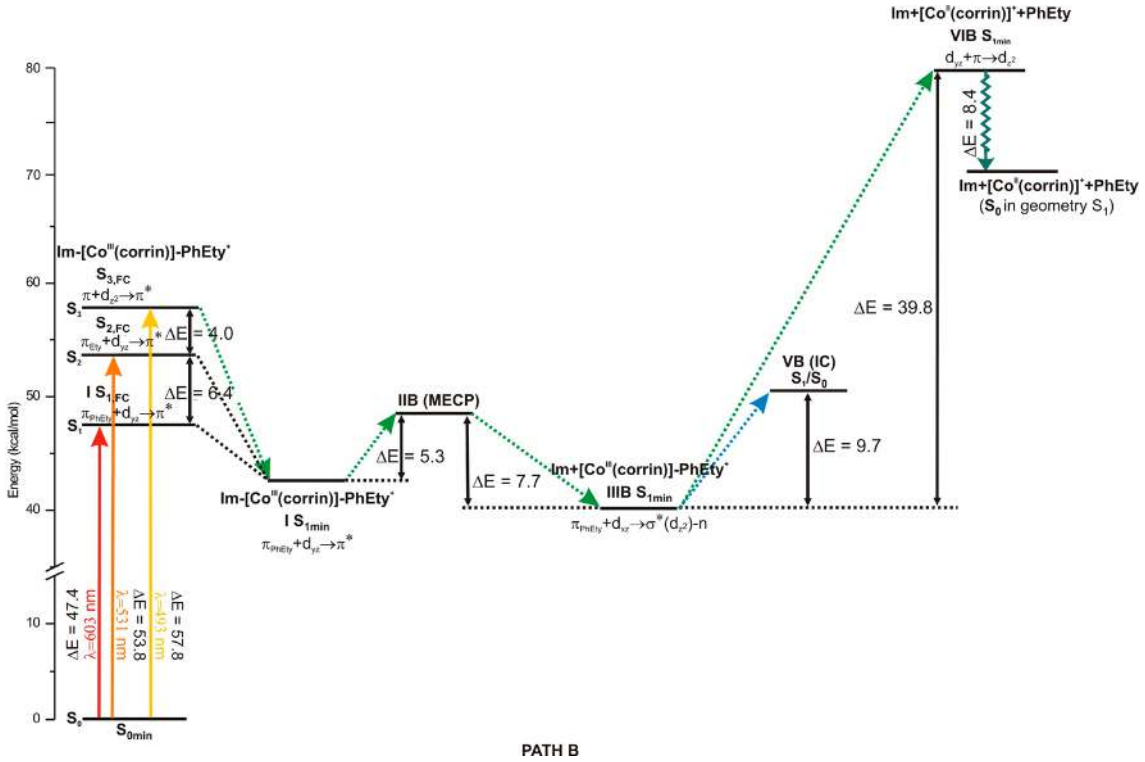

Figure 7. Energy diagram of photoreaction on path B for Im-[Co^{III}(corrin)]-PhEty^{+} model complex (ΔE values in kcal/mol).

3.7. PhEtyCbl PES. The PESs gathered in Figures 6 and S7 show the locations of the energy minima for the S_0, S_1, and S_2 electronic states of Im-[Co^{III}(corrin)]-PhEty^{+}. The relaxed S_1 PES indicate two regions that are low in energy and separated by a seam. The S_1 minima regions result from the interaction of at least two different electronic states. The region associated with shorter Co−C axial bond lengths corresponds to the MLCT transition, whereas the minimum associated with longer Co−C and Co−N_{Im} bonds corresponds to LF excitation. The first minimum is located in the area of the projection corresponding to shorter Co−C and Co−N_{Im} bond lengths and is denoted by the point I S_{1min}. The second low energy region is located in the region where Co−C distances are short (1.8−2.3 Å) and Co−N_{Im} distances are elongated (2.6−3.4 Å). Long Co−C bonds are associated with the high energy regions on the S_1 PES, and a steep increase in energy occurs as the Co−C bond is lengthened while the Co−N bond remains unperturbed.

The PES in Figure 6c shows several stationary points. The MLCT minimum is denoted I S_{1min}. IIB (MECP) denotes the minimum energy MLCT/LF crossing point of path B. In the LF region of the surface, the elongation of the Co−N_{Im} bond is associated with the detachment of the axial base from the cobalt center and point IIIB S_{1min} corresponds to a stable intermediate in the base-off form, which can undergo IC to S_0.

3.8. Ineffective Photodissociation and Energy Profiles of PhEtyCbl Photoreaction. For PhEtyCbl, as for parent CNCbl, photodissociation is not feasible from an experimental point of view.[15] We have corroborated this finding with our theoretical results for Im-[Co^{III}(corrin)]-PhEty^{+}. Like Im-[Co^{III}(corrin)]-EtPh^{+}, there are two possible routes for Co−C bond dissociation upon inspection of the S_1 PES (Figure 6c). Path A, which involves the elongation of the Co−C bond while the Co−N bond remains unchanged, is not energetically favorable. Conversely, path B is characterized by a low energy barrier between the MLCT and LF regions and thus it is significantly more energetically advantageous; however, this path will result in IC to S_0 and not in photodissociation. This path involves the elongation of the Co−N bond starting from the MLCT minimum (I S_{1min}, Figure 6) and proceeds through the seam at the MECP point until the system reaches the LF region. After crossing the IIB (MECP) point, on the surface of the LF electronic state, the relaxation to III B minimum occurs. Competition between two processes, i.e., IC and photodissociation from this minimum, is dependent upon the height of the energy barrier of these processes. In the case of the discussed complex, IC is the more favorable process.

The energetics for the photoreaction along path B for Im-[Co^{III}(corrin)]-PhEty^{+} are shown in Figure 7. There are some general similarities with the photoreaction of the Im-[Co^{III}(corrin)]-EtPh^{+} model complex, but the biggest differences are in the magnitude of the energies between the various points along the reaction pathway. The S_1 and S_2 states are populated upon excitation with a wavelength of 603 and 531 nm, respectively, whereby both excitations have small oscillator strength values. From among the remaining electronic states in the α/β region, S_3 is the most probable electronic state, which is populated during absorption at about 550 nm (calculated 493 nm). First, after the initial excitation, there is a relaxation to the MLCT minima, I S_{1min}, which is energetically favorable. To reach the MECP 5.3 kcal/mol of energy is required prior to reaching the second minima IIIB S_{1min}, in the LF region. From this point, there is a significant energetic preference for IC to S_0 instead of photodissociation. On the basis of our calculations, relaxation to S_0 from point IIIB S_{1min} requires overcoming a barrier equal to only 9.7 kcal/mol, whereas the calculated energy for photodissociation is about 39.8 kcal/mol (Figure 7).

DOI: 10.1021/acs.inorgchem.8b00956
Inorg. Chem. XXXX, XXX, XXX−XXX

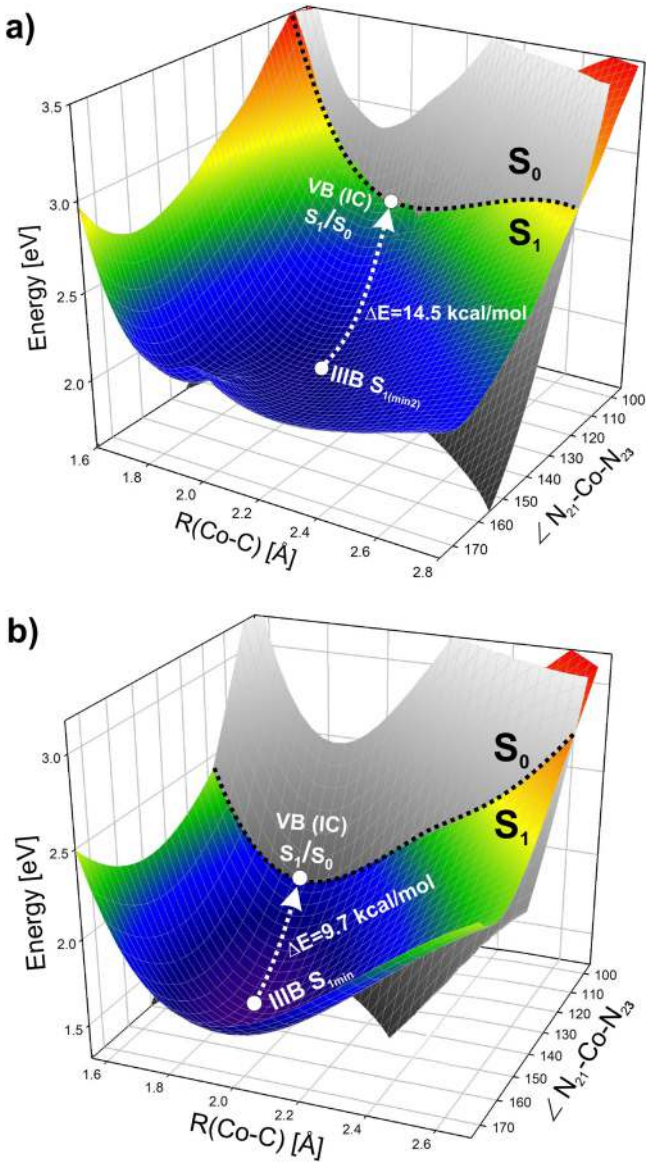

Figure 8. Potential energy surface for the S_1 optimized geometry as a function of Co−C bond length and N_{21}−Co−N_{23} valence angle with the minimum energy path for S_1/S_0 internal conversion depicted for (a) [Co^{III}(corrin)]-$EtPh^+$ and (b) [Co^{III}(corrin)]-$PhEty^+$ model complexes.

3.9. Mechanism of Internal Conversion. The mechanism for IC for the [Co^{III}(corrin)]-$EtPh^+$ and [Co^{III}(corrin)]-$PhEty^+$ can be understood using a PES constructed as a function of Co−C bond length and N_{21}−Co−N_{23} valence angle (Figure 8). The above mentioned model structures correspond to complexes with a fully detached axial base. Upon visual inspection of these PESs, it is apparent that the S_0 and S_1 surfaces cross. It is at this crossing that IC can occur. The minimum energy path for IC with [Co^{III}(corrin)]-$EtPh^+$ and [Co^{III}(corrin)]-$PhEty^+$ begins at point IIIB and proceeds to VB (IC) which is the point where the S_1 and S_0 surfaces cross. From IIIB $S_{1(min2)}$ to VB (IC), 14.5 kcal/mol is required to overcome the barrier for IC in the case of the [Co^{III}(corrin)]-$EtPh^+$ complex. The IC process for the second antivitamin, [Co^{III}(corrin)]-$PhEty^+$, is more energetically favorable than for [Co^{III}(corrin)]-$EtPh^+$ as only 9.7 kcal/mol is required from the first point to the second on the path of minimal energy.

Deactivation can be further considered upon inspection of the PECs in Figure 9. These PECs correspond to geometries where the axial base is fully detached and they are extrapolations of the PESs in Figures 4c and 6c. For [Co^{III}(corrin)]-$EtPh^+$, Figure 9a, it is apparent from the S_1 curve that the photochemical reaction takes place essentially barrierless between the crossing of the two electronic states, MLCT and LF. For [Co^{III}(corrin)]-$PhEty^+$ (Figure 9b), the crossing of states for [Co^{III}(corrin)]-$EtPh^+$, is not observed. This is to be expected as the seam for the PES corresponding to the photodissociation (Figure 6c) is not as distinctive. It is also of note that the excitation to the S_1 curve for [Co^{III}(corrin)]-$PhEty^+$ (∼1.40 eV), is much lower in energy than [Co^{III}(corrin)]-$EtPh^+$ (∼2.1 eV). There is a gap between the S_0 curves and the S_1 curve for [Co^{III}(corrin)]-$EtPh^+$ whereas for [Co^{III}(corrin)]-$PhEty^+$ there is a very minimal gap between the S_0 and S_1 curves at bond distances greater than 2.6 Å. The small energetic difference between the S_0 and S_1 curves for [Co^{III}(corrin)]-$PhEty^+$ further corroborate the preference for IC. In fact, this is quite similar to CNCbl and HOCbl, where the S_0 and S_1 PESs nearly meet at long bond distances.[27] The PECs for [Co^{III}(corrin)]-$EtPh^+$ are more similar to the PESs of the photolabile MeCbl and AdoCbl, where a gap in energy remains between the S_0 and S_1 surfaces, even when the axial bonds are elongated.[27] This gap in energy between the S_0 and S_1 curves for [Co^{III}(corrin)]-$EtPh^+$ are further evidence of the potential for photodissociation for this conditional antivitamin B_{12}.

4. SUMMARY AND CONCLUSIONS

When photochemistry of EtPhCbl is compared to alkylcobalamins such as MeCbl or AdoCbl, which have been thoroughly investigated both experimentally as well as theoretically, one can conclude that EtPhCbl behaves more like cobalamins that are in base-off configurations.[15,27−29,31] However, unlike MeCbl or AdoCbl, when EtPhCbl is excited in the visible or near-UV regions, significant dissociation of the upper axial ligand is not observed. The absorption spectrum of the excited state indicates a LF minimum with a dissociated lower axial ligand as well as an elongated Co−C bond to the upper axial ligand. In addition, transient absorption measurements indicate that the lower axial ligand (DBI) is photodetached.[15] PECs for the optimized geometries of S_1 (Figure 9) that correspond to the base-off form confirm these experimental results. The S_1 PEC, which is an extrapolation of the PES in the dissociation limit of axial base (Figure 4c), indicates that the intersection between the MLCT and LF electronic states is essentially barrierless, and the photoreaction proceeds through the LF region as the Co−C bond undergoes elongation. Experimental results also indicate that IC is observed for EtPhCbl and that a long-lived base-off product is formed.[15] This is a distinct difference in comparison to other cobalamins such as MeCbl or HOCbl, where IC between excited states is not observed.[27,49] Our theoretical results validate the categorization of EtPhCbl as a conditional antivitamin B_{12} as we have determined an optimum pathway (path B) for photolysis (Figures 4 and 5).

The major conclusion associated with PhEtyCbl's photolytic properties is that it is incredibly photostable. Transient absorption measurements indicate that upon excitation PhEtyCbl experiences IC to S_0 with a quantum yield of essentially one. Photoproducts are not detected in such measurements.[15] Our results indicate that from the minimum of the LF electronic excited state there is a substantial energetic

DOI: 10.1021/acs.inorgchem.8b00956
Inorg. Chem. XXXX, XXX, XXX−XXX

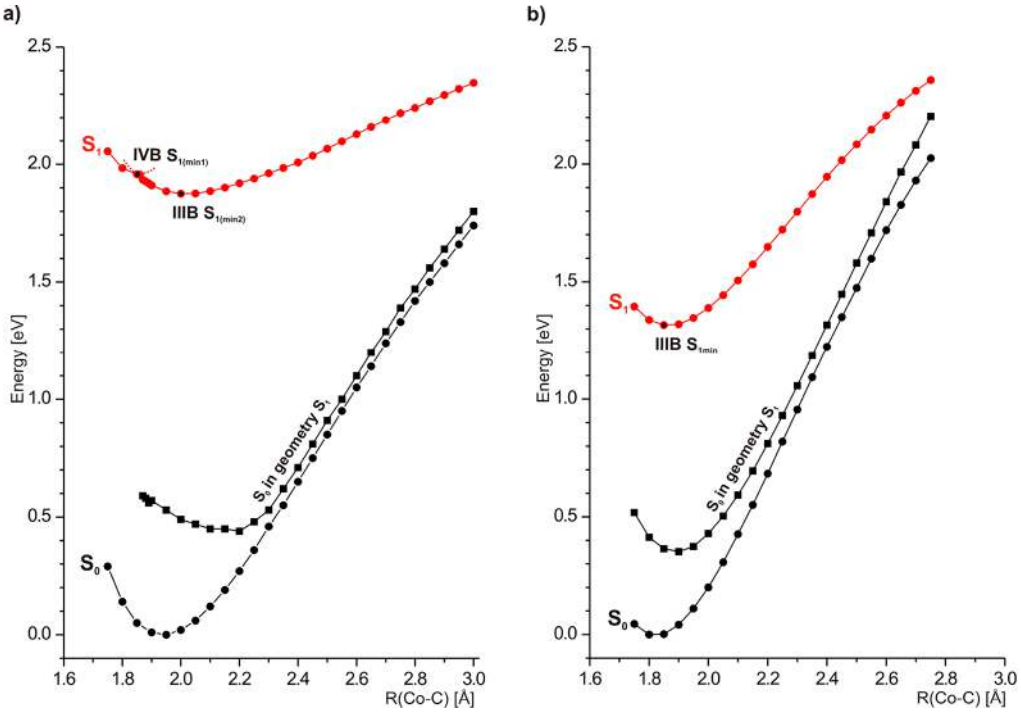

Figure 9. Potential energy curves (PECs) for optimized geometries of S_1 state as function Co−C bond length for (a) [Co^{III}(corrin)]-$EtPh^+$ and (b) [Co^{III}(corrin)]-$PhEty^+$ model complexes.

barrier of 39.8 kcal/mol in order for photodissociation to occur via path B, whereas the energetic barrier for IC is only 9.7 kcal/mol (Figure 7). Sension and co-workers estimated the activation barrier for IC to the S_0 for PhEtyCbl in solution to be ∼12.6 kJ/mol (∼3.0 kcal/mol) using an Arrhenius Plot.[15] This is higher than the IC barrier for CNCbl in solution ∼8.8 kJ/mol (∼2.0 kcal/mol).[39] In previous studies, we have estimated the energy barrier for IC to be 5.0 kcal/mol for a truncated model of CNCbl.[32] The calculated barrier for Im-[Co^{III}(corrin)]-$PhEty^+$ is 9.7 kcal/mol, so these theoretical results corroborate the experimental observation that the energetic barrier for internal conversion S_1/S_0 is greater than that for PhEtyCbl than CNCbl. The Co−C bond (1.86 Å) in PhEtyCbl is shorter than those of other cobalamins and is sp-hybridized. As a result, the Co−C_{sp} bond is stronger than that of other alkyl cobalamins such as AdoCbl.[9] In addition to photostability, it is also resistant to thermal cleavage of the Co−C bond.

In conclusion, we have provided a theoretical analysis of the photolytic properties of two newly characterized non-natural cobalamins. These theoretical results provide insights into the electronic structure of the lowest excited state, which directly determines photolability and conversely photostability of the investigated antivitamins. There are two pathways for photolysis, and based on energetics, an optimum path can be determined. EtPhCbl (Im-[Co^{III}(corrin)]-$EtPh^+$) can photodissociate via path B through the LF state with a substantially elongated axial base, although the quantum yield of photoproducts is low. Similarly for PhEtyCbl (Im-[Co^{III}(corrin)]-$PhEty^+$), two pathways can be identified; however, neither are energetically feasible for Co−C bond photolysis, thus explaining the incredible photostability of this antimetabolite. These results for the model complexes have important implications for understanding experimental results. As a result of the overwhelming energetic favorability for IC, PhEtyCbl is photostable. In contrast, for EtPhCbl, there is a competition of sorts between IC and photodissociation as the energetic barriers are comparable. It is not surprising that EtPhCbl and PhEtyCbl both exhibit difficulty in dissociating the upper axial ligand as these cobalamins have been shown to be metabolically inert. Photohomolysis of the Co−C bond will result in a photoactive metabolite with potential medicinal applications. In addition, the results gathered in this study are of particular importance especially as more applications for synthetic vitamin-B_{12} derivatives continue to be realized.

■ ASSOCIATED CONTENT

Supporting Information

The Supporting Information is available free of charge on the ACS Publications website at DOI: 10.1021/acs.inorgchem.8b00956.

Selected optimized geometric parameters for investigated complexes (Im-[Co^{III}(corrin)]-$EtPh^+$, [Co^{III}(corrin)]-$EtPh^+$, Im-[Co^{III}(corrin)]-$PhEty^+$, and [Co^{III}(corrin)]-$PhEty^+$), TD-DFT excitation energies, oscillator strengths, composition and characters of singlet electronic transitions for base-on and base-off forms of model complexes, chemical structures, optimized geometries in ground state S_0 and in excited state S_1, selected molecular orbitals involved in vertical electronic excitations, potential energy surfaces for ground state and first, vertical excited state, orbital energy diagram for ground states, and first excited states for molecular orbitals of EtPhCbl and PhEtyCbl structural models (PDF)

■ AUTHOR INFORMATION

Corresponding Author

*Phone: (502) 852-6609. Fax: (502) 852-8149. E-mail: pawel@louisville.edu.

DOI: 10.1021/acs.inorgchem.8b00956
Inorg. Chem. XXXX, XXX, XXX−XXX

ORCID

Pawel M. Kozlowski: 0000-0002-4090-8078

Notes

The authors declare no competing financial interest.

■ ACKNOWLEDGMENTS

This work was supported by the National Science Centre Poland (UMO-2015/17/B/ST4/03733). The TURBOMOLE calculations were carried out in the Wrocław Centre for Networking and Supercomputing, WCSS, Wrocław, Poland, http://www.wcss.wroc.pl, under computational Grant No. 18.

■ REFERENCES

(1) Zelder, F. Recent Trends in the Development of Vitamin B_{12} Derivatives for Medicinal Applications. *Chem. Commun. (Cambridge, U. K.)* **2015**, *51*, 14004−14017.
(2) Kräutler, B. Antivitamins B_{12}−A Structure and Reactivity-Based Concept. *Chem. - Eur. J.* **2015**, *21*, 11280−11287.
(3) Somogyi, J. C. *Results of Basic Medical Research* **1956**, *1*, 139−188.
(4) Zelder, F.; Sonnay, M.; Prieto, L. Antivitamins for Medicinal Applications. *ChemBioChem* **2015**, *16*, 1264−1278.
(5) Freedman, M. D. Warfarin and Other "Anti"-Vitamin K Anticoagulants: Pharmacodynamics and Clinical Use. *Am. J. Ther.* **1996**, *3*, 771−783.
(6) Hirsh, J.; O'Donnell, M.; Eikelboom, J. W. Beyond Unfractionated Heparin and Warfarin. *Circulation* **2007**, *116*, 552−560.
(7) Zhou, K.; Oetterli, R. M.; Brandl, H.; Lyatuu, F. E.; Buckel, W.; Zelder, F. Chemistry and Bioactivity of an Artificial Adenosylpeptide B_{12} Cofactor. *ChemBioChem* **2012**, *13*, 2052−2055.
(8) Zhou, K.; Zelder, F. Vitamin B12 Mimics Having a Peptide Backbone and Tuneable Coordination and Redox Properties. *Angew. Chem., Int. Ed.* **2010**, *49*, 5178−5180.
(9) Ruetz, M.; Gherasim, C.; Gruber, K.; Fedosov, S.; Banerjee, R.; Kräutler, B. Access to Organometallic Arylcobaltcorrins Through Radical Synthesis: 4-Ethylphenylcobalamin, a Potential "Antivitamin B_{12}". *Angew. Chem., Int. Ed.* **2013**, *52*, 2606−2610.
(10) Ruetz, M.; Salchner, R.; Wurst, K.; Fedosov, S.; Kräutler, B. Phenylethynylcobalamin: A Light-Stable and Thermolysis-Resistant Organometallic Vitamin B_{12} Derivative Prepared by Radical Synthesis. *Angew. Chem., Int. Ed.* **2013**, *52*, 11406−11409.
(11) Banerjee, R.; Gherasim, C.; Padovani, D. The Tinker, Tailor, Soldier in Intracellular B_{12} Trafficking. *Curr. Opin. Chem. Biol.* **2009**, *13*, 484−491.
(12) Dolphin, D. *B_{12} Vol. 1: Chemistry*; John Wiley & Sons, New York, 1982; Vol. *1*.
(13) Banerjee, R. *Chemistry and Biochemistry of B_{12}*; Wiley: New York, 1999.
(14) Mutti, E.; Ruetz, M.; Birn, H.; Kräutler, B.; Nexo, E. 4-Ethylphenyl-Cobalamin Impairs Tissue Uptake of Vitamin B_{12} and Causes Vitamin B_{12} Deficiency in Mice. *PLoS One* **2013**, *8*, e75312.
(15) Miller, N. A.; Wiley, T. E.; Spears, K. G.; Ruetz, M.; Kieninger, C.; Kräutler, B.; Sension, R. J. Toward the Design of Photoresponsive Conditional Antivitamins B_{12}: A Transient Absorption Study of an Arylcobalamin and an Alkynylcobalamin. *J. Am. Chem. Soc.* **2016**, *138*, 14250−14256.
(16) Lodowski, P.; Ciura, K.; Toda, M. J.; Jaworska, M.; Kozlowski, P. M. Photodissociation of Ethylphenylcobalamin Antivitamin B_{12}. *Phys. Chem. Chem. Phys.* **2017**, *19*, 30310−30315.
(17) Runge, E.; Gross, E. K. U. Density-Functional Theory for Time-Dependent Systems. *Phys. Rev. Lett.* **1984**, *52*, 997−1000.
(18) Casida, M. E. *Recent Developments and Application of Modern Density Functional Theory*; Elsvevier: Amsterdam, 1996; pp 391−439.
(19) Sierka, M.; Hogekamp, A.; Ahlrichs, R. Fast Evaluation of the Coulomb Potential for Electron Densities using Multipole Accelerated Resolution of Identity Approximation. *J. Chem. Phys.* **2003**, *118*, 9136−9148.
(20) Becke, A. D. Density-Functional Exchange-Energy Approximation with Correct Asymptotic Behavior. *Phys. Rev. A: At., Mol., Opt. Phys.* **1988**, *38*, 3098−3100.
(21) Perdew, J. P. Density-Functional Approximation for the Correlation Energy of the Inhomogeneous Electron Gas. *Phys. Rev. B: Condens. Matter Mater. Phys.* **1986**, *33*, 8822−8824.
(22) Weigend, F.; Häser, M.; Patzelt, H; Ahlrichs, R. RI-MP2: Optimized Auxiliary Basis Sets and Demonstration of Efficiency. *Chem. Phys. Lett.* **1998**, *294*, 143−152.
(23) Eichkorn, K.; Weigend, F.; Treutler, O.; Ahlrichs, R. Auxiliary Basis Sets for Main Row Atoms and Transition Metals and their use to Approximate Coulomb Potentials. *Theor. Chem. Acc.* **1997**, *97*, 119−124.
(24) Klamt, A.; Schuurmann, G. COSMO: A New Approach to Dielectric Screening in Solvents with Explicit Expressions for the Screening Energy and its Gradient. *J. Chem. Soc., Perkin Trans. 2* **1993**, *2*, 799−805.
(25) Ahlrichs, R.; Bär, M.; Baron, H. P.; Bauernschmitt, R.; Böcker, S.; Crawford, N.; Deglmann, P.; Ehrig, M.; Eichkorn, K.; Elliott, S.; Furche, F.; Haase, F.; Häser, M.; Hättig, C.; Hellweg, A.; Horn, H.; Huber, C.; Huniar, U.; Kattannek, M.; Köhn, A.; Kölmel, C.; Kollwitz, M.; May, K. S.; Nava, P.; Ochsenfeld, C.; Öhm, H.; Patzelt, H.; Rappoport, D.; Rubner, O.; Schäfer, A.; Schneider, U.; Sierka, M.; Treutler, O.; Unterreiner, B.; von Arnim, M.; Weigend, F.; Weis, P.; Weiss, H. *TURBOMOLE*; Quantum Chemistry Group, University of Karlsruhe, Germany, 1988. http://www.turbomole.com.
(26) Schmidt, M. W.; Baldridge, K. K.; Boatz, J. A.; Elbert, S. T.; Gordon, M. S.; Jensen, J. H.; Koseki, S.; Matsunaga, N.; Nguyen, K. A.; Su, S.; et al. General Atomic and Molecular Electronic Structure System. *J. Comput. Chem.* **1993**, *14*, 1347−1363.
(27) Kozlowski, P. M.; Garabato, B. D.; Lodowski, P.; Jaworska, M. Photolytic Properties of Cobalamins: A Theoretical Perspective. *Dalton Trans.* **2016**, *45*, 4457−4470.
(28) Lodowski, P.; Jaworska, M.; Andruniow, T.; Garabato, B. D.; Kozlowski, P. M. Mechanism of Co-C Bond Photolysis in the Base-on Form of Methylcobalamin. *J. Phys. Chem. A* **2014**, *118*, 11718−11734.
(29) Lodowski, P.; Jaworska, M.; Garabato, B. D.; Kozlowski, P. M. Mechanism of Co-C Bond Photolysis in Methylcobalamin: Influence of Axial Base. *J. Phys. Chem. A* **2015**, *119*, 3913−3928.
(30) Garabato, B. D.; Kumar, N.; Lodowski, P.; Jaworska, M.; Kozlowski, P. M. Electronically Excited States of Cob(II)alamin: Insights from CASSCF/XMCQDPT2 and TD-DFT calculations. *Phys. Chem. Chem. Phys.* **2016**, *18*, 4513−4526.
(31) Garabato, B. D.; Lodowski, P.; Jaworska, M.; Kozlowski, P. M. Mechanism of Co-C Photodissociation in Adenosylcobalamin. *Phys. Chem. Chem. Phys.* **2016**, *18*, 19070−19082.
(32) Lodowski, P.; Jaworska, M.; Andruniow, T.; Garabato, B. D.; Kozlowski, P. M. Mechanism of the S_1 Excited State Internal Conversion in Vitamin B_{12}. *Phys. Chem. Chem. Phys.* **2014**, *16*, 18675−18679.
(33) Kornobis, K.; Kumar, N.; Lodowski, P.; Jaworska, M.; Piecuch, P.; Lutz, J. J.; Wong, B. M.; Kozlowski, P. M. Electronic Structure of the S_1 State in Methylcobalamin: Insight from CASSCF/MC-XQDPT2, EOM-CCSD, and TD-DFT Calculations. *J. Comput. Chem.* **2013**, *34*, 987−1004.
(34) Kornobis, K.; Kumar, N.; Wong, B. M.; Lodowski, P.; Jaworska, M.; Andruniow, T.; Ruud, K.; Kozlowski, P. M. Electronically Excited States of Vitamin B_{12}: Benchmark Calculations Including Time-Dependent Density Functional Theory and Correlated *ab initio* Methods. *J. Phys. Chem. A* **2011**, *115*, 1280−1292.
(35) Kornobis, K.; Ruud, K.; Kozlowski, P. M. Cob(I)alamin: Insight into the Nature of Electronically Excited States Elucidated via Quantum Chemical Computations and Analysis of Absorption, CD, and MCD data. *J. Phys. Chem. A* **2013**, *117*, 863−876.
(36) Walker, L. A.; Jarrett, J. T.; Anderson, N. A.; Pullen, S. H.; Matthews, R. G.; Sension, R. J. Time-Resolved Spectroscopic Studies of B_{12} Coenzymes: The Identification of a Metastable Cob(III)alamin Photoproduct in the Photolysis of Methylcobalamin. *J. Am. Chem. Soc.* **1998**, *120*, 3597−3603.

DOI: 10.1021/acs.inorgchem.8b00956
Inorg. Chem. XXXX, XXX, XXX−XXX

(37) Shiang, J. J.; Walker, L. A.; Anderson, N. A.; Cole, A. G.; Sension, R. J. Time-Resolved Spectroscopic Studies of B_{12} Coenzymes: The Photolysis of Methylcobalamin is Wavelength Dependent. *J. Phys. Chem. B* **1999**, *103*, 10532−10539.
(38) Cole, A. G.; Yoder, L. M.; Shiang, J. J.; Anderson, N. A.; Walker, L. A.; Banaszak Holl, M. M.; Sension, R. J. Time-Resolved Spectroscopic Studies of B_{12} Coenzymes: A Comparison of the Primary Photolysis Mechanism in Methyl-, Ethyl-, n-Propyl-, and 5'-Deoxyadenosylcobalamin. *J. Am. Chem. Soc.* **2002**, *124*, 434−441.
(39) Harris, D. A.; Stickrath, A. B.; Carroll, E. C.; Sension, R. J. Influence of Environment on the Electronic Structure of Cob(III)-alamins: Time-Resolved Absorption Studies of the S1 State Spectrum and Dynamics. *J. Am. Chem. Soc.* **2007**, *129*, 7578−7585.
(40) Peach, M. J.; Benfield, P.; Helgaker, T.; Tozer, D. J. Excitation Energies in Density Functional Theory: An Evaluation and a Diagnostic Test. *J. Chem. Phys.* **2008**, *128*, 044118.
(41) Stich, T. A.; Brooks, A. J.; Buan, N. R.; Brunold, T. C. Spectroscopic and Computational Studies of Co^{3+}-Corrinoids: Spectral and Electronic Properties of the B_{12} Cofactors and Biologically Relevant Precursors. *J. Am. Chem. Soc.* **2003**, *125*, 5897−5914.
(42) Toohey, J. I. A. Vitamin B_{12} Compound Containing No Cobalt. *Proc. Natl. Acad. Sci. U. S. A.* **1965**, *54*, 934−942.
(43) Pratt, J. M. *Inorganic Chemistry of Vitamin B_{12}*; Academic Press: London, 1972.
(44) Wiley, T. E.; Arruda, B. C.; Miller, N. A.; Lenard, M.; Sension, R. J. Excited Electronic States and Internal Conversion in Cyanocobalamin. *Chin. Chem. Lett.* **2015**, *26*, 439−443.
(45) Andruniów, T.; Jaworska, M.; Lodowski, P.; Zgierski, M. Z.; Dreos, R.; Randaccio, L.; Kozlowski, P. M. Time-Dependent Density Functional Theory Study of Cobalt Corrinoids: Electronically Excited States of Methylcobalamin. *J. Chem. Phys.* **2008**, *129*, 085101.
(46) Miller, N. A.; Deb, A.; Alonso-Mori, R.; Garabato, B. D.; Glownia, J. M.; Kiefer, L. M.; Koralek, J.; Sikorski, M.; Spears, K. G.; Wiley, T. E.; Zhu, D.; Kozlowski, P. M.; Kubarych, K. J.; Penner-Hahn, J. E.; Sension, R. J. Polarized XANES Monitors Femtosecond Structural Evolution of Photoexcited Vitamin B_{12}. *J. Am. Chem. Soc.* **2017**, *139*, 1894−1899.
(47) Peng, J.; Tang, K.-C.; McLoughlin, K.; Yang, Y.; Forgach, D.; Sension, R. J. Ultrafast Excited-State Dynamics and Photolysis in Base-Off B_{12} Coenzymes and Analogues: Absence of the trans-Nitrogenous Ligand Opens a Channel for Rapid Nonradiative Decay. *J. Phys. Chem. B* **2010**, *114*, 12398−12405.
(48) Jones, A. R.; Woodward, J. R.; Scrutton, N. S. Continuous Wave photolysis Magnetic Field Effect Investigations with Free and Protein-Bound Alkylcobalamins. *J. Am. Chem. Soc.* **2009**, *131*, 17246−17253.
(49) Wiley, T. E.; Miller, W. R.; Miller, N. A.; Sension, R. J.; Lodowski, P.; Jaworska, M.; Kozlowski, P. M. Photostability of Hydroxocobalamin: Ultrafast Excited State Dynamics and Computational Studies. *J. Phys. Chem. Lett.* **2016**, *7*, 143−147.

DOI: 10.1021/acs.inorgchem.8b00956
Inorg. Chem. XXXX, XXX, XXX−XXX